九州大学学術情報リポジトリ
Kyushu University Institutional Repository

Switching Between Continuum and Discrete States in a Continuum Robot With Dislocatable Joints

Kanada, Ayato
Department of Mechanical Engineering, Kyushu University

Mashimo, Tomoaki
Department of Mechanical Engineering, Toyohashi University of Technology

https://hdl.handle.net/2324/7172163

出版情報：IEEE Access. 9, pp.34859-34867, 2021-02-26. Institute of Electrical Electronics Engineers (IEEE)
バージョン：
権利関係：Creative Commons Attribution 4.0 International

KYUSHU UNIVERSITY

IEEE Access
Multidisciplinary | Rapid Review | Open Access Journal

Received January 29, 2021, accepted February 21, 2021, date of publication February 26, 2021, date of current version March 5, 2021.

Digital Object Identifier 10.1109/ACCESS.2021.3062284

Switching Between Continuum and Discrete States in a Continuum Robot With Dislocatable Joints

AYATO KANADA[1], (Member, IEEE), AND TOMOAKI MASHIMO[2], (Member, IEEE)
[1]Department of Mechanical Engineering, Kyushu University, Fukuoka 819-0395, Japan
[2]Department of Mechanical Engineering, Toyohashi University of Technology, Toyohashi 441-8580, Japan

Corresponding author: Ayato Kanada (kanada@mech.kyushu-u.ac.jp)

This work was supported in part by the Grant-in-Aid for Research Activity Start-up under Grant 20K22398.

ABSTRACT Rigid linkages allow robots to lift heavy loads but prevent them from gently stretching and bending their bodies. Continuum robots without rigid linkages have a wide range of motion, safety, shape adaptability, and compliance. To combine the benefits of both continuum and rigid robots, we propose a method of switching between discrete and continuum states by a dislocatable joint. This mechanism is driven by three wires. It has a cup joint in an upper section and a ball joint in a lower section, and the two sections are connected by a spring. The cup and ball joints are separated, and the manipulator is a flexible continuum one. When the wires through the sections are pulled, the two joints are connected as a discrete state. To clarify the design methodology of the manipulator, we build a model of the joint and consider three collision cases in the simulation and experiment. The model reveals the relationship between the robot's shape parameters and the manipulator's range of motion, and it visualizes an area where the positioning is uncertain due to the collision between the ball and cup joints. We build a prototype manipulator and experimentally verify that the stiffness is improved by the connection.

INDEX TERMS Continuum robots, discrete robots, dislocatable joints, variable stiffness.

I. INTRODUCTION

Conventional industrial robots require a high level of stiffness to execute tasks with agility and accuracy in manufacturing. These robots are actuated in confined spaces separately from workers because of their use of rigid linkages, which enable them to handle heavy load tasks. Manipulators using elastic components, e.g., series elastic actuators [1], have been deemed safe and have contributed to work in close proximity with humans in factories [2], [3]. Continuum robots, which are continuously curved manipulators that are flexible and compliant, are examples of safe robots. Soft continuum robots are inherently safe because of soft and lightweight structures that are either wire driven [4]–[6] or pneumatically controlled [7]–[9]. High flexibility is a considerable advantage but reduces accuracy and payload.

Variable stiffness mechanisms have much potential for applications that require safety and large payloads. Granular jamming is a well-known variable stiffness mechanism applied to continuum robots [10]–[14]. In this mechanism, an elastic membrane is filled with small particles to increase the stiffness of a robot's body. In the neutral state, the particles are free and movable, and external forces can deform the links. The air inside the elastic membrane is sucked, thereby inhibiting particle movement and stiffening the robot. When the negative air pressure is released, the particles regain their movability. This idea is simple and easy to build, but the robot cannot operate during the suction due to the friction between the particles. Functional materials, such as magnetorheology and electrorheology materials (which can modify an object's rheological properties [15]–[17]) and low-melting-point materials (which dramatically reduce the stiffness) [18], [19], are also used to alter the stiffness. However, they require tight fluidic channels for the liquids and gases. Another interesting methodology is antagonistic action. One example is a combination of McKibben actuators that operate in different directions [20]. They comprise a flexible pneumatic chamber wrapped in a braided structure that either expands or contracts by changing the angle between the fibers of the braided structure and the axis of

The associate editor coordinating the review of this manuscript and approving it for publication was Yingxiang Liu.

This work is licensed under a Creative Commons Attribution 4.0 License. For more information, see https://creativecommons.org/licenses/by/4.0/

the actuator. The McKibben actuators act antagonistically to increase stiffness by coupling their extension and contraction. They can change the stiffness by the magnitude of the pressure, but the complicated structure makes the control difficult.

In nature, animals can change their body stiffness [21]. For example, vertebrates change their stiffness by antagonizing their muscles through their joints. They are similar to conventional rigid robots, which transmit high power through discrete joints. Other examples are invertebrates, which do not have rigid bones, such as sea cucumbers and starfish. Similar to continuum robots, they have small bone fragments scattered on the surface of their bodies and in their arms. They can change their rigidity and range of motion by altering the stiffness of the elastic connective tissue (catch connective tissue) that connects their bone fragments [22], [23].

Vertebrates have relatively high payloads, but they do not actively disengage their joints. Exceptionally, snakes can separate their jaws to open their mouth widely and have highly mobile jaw joints, whose left and right anterior ends are joined by a flexible ligament [24]. Inspired by these animals and biology, we propose a concept for a variable stiffness manipulator that can shift between discrete and continuum states by dislocatable joints. Fig. 1 (a) shows a schematic of the proposed joint mechanism driven by three wires. The upper section has a cup joint, and the lower section has a ball joint; the two sections are connected by a spring. When the three wires through the sections are strongly pulled, the cup and ball joints are connected, and the manipulator shifts from the continuum state to the discrete state (Fig. 1 (b)). A state can be selected by controlling the displacement and tension of the wires. This design has the advantages of both continuum and rigid robots. The continuum manipulator has a wide range of motion and high flexibility, and the discrete manipulator has high accuracy and a large payload.

Unlike fully soft robots, a certain type of soft robots with rigid mechanical elements shows a higher payload and better responsiveness, but the dislocatable joints that we propose in this paper have not been reported [25]. As an exception, a robotic arm that passively dislocates joints to absorb unexpected impacts has been reported [26], but has not dealt with continuum state and flexibility control.

In this paper, we examine the design and payload of the proposed variable stiffness manipulator with a dislocatable joint. Section II examines the collision condition of the joints and builds the model that can estimate collisions occurring in the proposed manipulator. Section III shows the maximum bending radius given changes in the design parameters. In Section IV, we build a prototype of the manipulator and experimentally verify the three collision models and the change in the stiffness. The primary contributions of this work are:

- A method for designing and fabricating of a continuum robot with dislocatable joints.

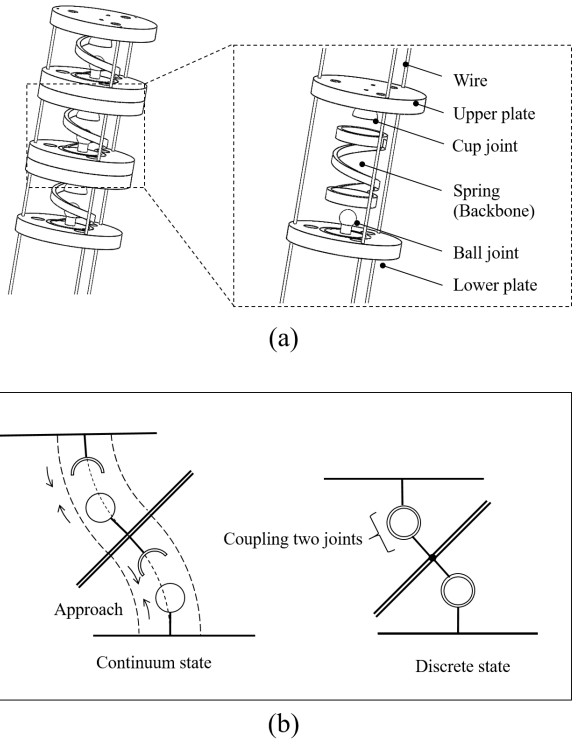

FIGURE 1. (a) Schematic of the proposed variable stiffness manipulator with a dislocatable joint. (b) Schematic of the joint dislocation mechanism.

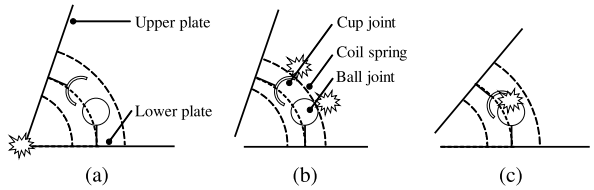

FIGURE 2. Three collision types occurring in the proposed manipulator: (a) plate and plate, (b) joint and spring, and (c) ball and cup joints.

- Modeling and validation of the collision model between continuum state and discrete state.
- Demonstration of the prototype manipulator in heavy object lifting.

II. KINEMATIC MODELING

Considering the collision between components is important for the kinematic design of the variable stiffness manipulator. Three types of collisions occur in the joint mechanism: (i) plate and plate, (ii) joint and spring, and (iii) ball and cup joints, as shown in Fig. 2 (a), (b), and (c), respectively. Planar models can be used to describe the system.

A. PLATE AND PLATE

We describe the collision between the upper and lower sections of the joint. Fig. 3 shows the continuum and discrete states of the sections. In this figure, L and λ are the lengths and the radii of an arc, respectively, when the bending angles θ_c and θ_d are given. When the upper section inclines and

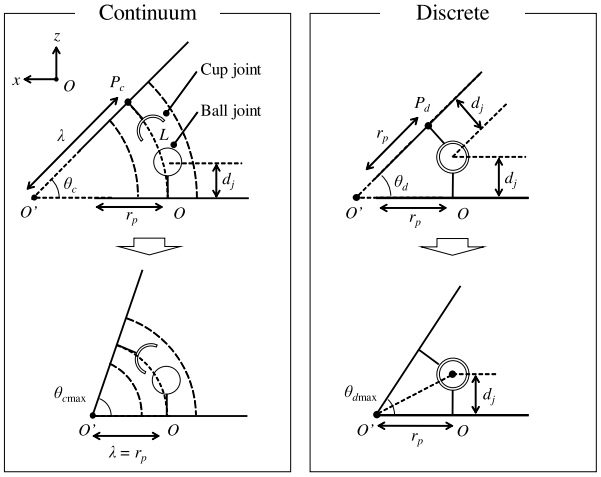

FIGURE 3. Collision between the upper and lower plates in the continuum and discrete states.

the angles θ_c and θ_d enlarge, the plate of the upper section collides with the lower plate. The angles between the upper and lower plates are denoted as the maximum bending angles θ_{cmax} and θ_{dmax}. We can calculate the two maximum bending angles geometrically. The constant curvature model is a well-known forward kinematics formula for continuum robots [27]. This model approximates the continuum sections using the parameters L, λ, and θ_c.

$$\lambda = \frac{L}{\theta_c} \tag{1}$$

In the continuum state, the coordinates of the end position P_c are as follows:

$$P_c(x, z) = (\lambda(1 - \cos\theta_c), \lambda \sin\theta_c) \tag{2}$$

In the discrete state, the coordinates of the end position P_d are as follows:

$$P_d(x, z) = (d_j \sin\theta_d, d_j(1 + \cos\theta_d)) \tag{3}$$

where d_j is the distance from the section plate to the center of the ball or cup. The collision between the two plates prevents the robot from bending. In the continuum state, the bending angle θ_c increases at a constant arc length L, and the radius λ decreases. When the plate's edges contact each other, the radius λ becomes equal to the length r_p between the plate edge and the original point O. The maximum bending angle θ_{cmax} is defined as follows:

$$\theta_{cmax} = \frac{L}{r_p} \tag{4}$$

In the discrete state, the upper plate inclines, and the two plates contact each other. The maximum bending angle θ_{dmax} is determined using the following equation:

$$\theta_{dmax} = 2 \arctan \frac{d_j}{r_p} \tag{5}$$

Equations (4) and (5) show that a larger range of motion is obtained at a larger distance between the two plates or a smaller plate diameter.

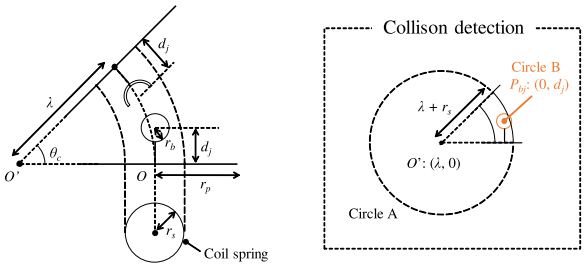

FIGURE 4. Collision between the joint and spring inner wall in the continuum state.

B. JOINT AND SPRING

We consider the collision between the outside of the ball or cup joint and the inside of the coil spring (Fig. 4). The diameter $2r_b$ of the ball or cup joint must be smaller than the inner diameter $2r_s$ of the coil spring. Whether the collision occurs depends on the bending angle. As the upper plate inclines and the bending angle θ_c increases, the joint collides with the inside of the coil spring, as shown in the left part of Fig. 4. We define a circle A with a center O' and radius $\lambda + r_s$ for the coil spring and a circle B with a center P_{bj} and radius r_{bj} for the ball joint, as shown in the right part of Fig. 4. This definition enables the use of circle-to-circle collision detection formulas, which are widely used in video games and other physical simulations. When the distance between the centers of circles A and B is larger than the difference between the radii of A and B, the two circles collide. The center coordinates of circles A and B are defined as (x_A, y_A) and (x_B, y_B), respectively, and the radii of circles A and B are r_A and r_B (where $r_A > r_B$), respectively. The collision detection is described as follows:

$$(x_A - x_B)^2 + (y_A - y_B)^2 \geq (r_A - r_B)^2 \tag{6}$$

Hence, we obtain the following equation from the coordinates and design of the coil spring and ball joint:

$$(\lambda - 0)^2 + (0 - d_j)^2 \geq (\lambda + r_s - r_b)^2 \tag{7}$$

In (4), (5), and (7), there is a trade-off between the plate-to-plate collision and joint-to-spring collision in the joint parameters. For example, in the plate-to-plate collision expressed in (4) and (5), a larger d_j and a smaller r_p enlarge the range of motion. On the contrary, in the joint-to-spring collision expressed in (7), a smaller d_j and a larger r_s enlarge the range of motion (From $r_s < r_p$, The larger r_p, the larger r_s can be).

C. BALL AND CUP JOINT

We consider the collision between the ball and the edge of the cup joints in Fig. 5. The cup joint is attached to the lower section plate, and the ball joint is attached to the upper one, as shown in the left part of Fig. 5. The ball and cup joints are denoted as a circle and a semicircle, respectively, with the same radius r_b. The coordinate P_{bj} of the ball joint is given

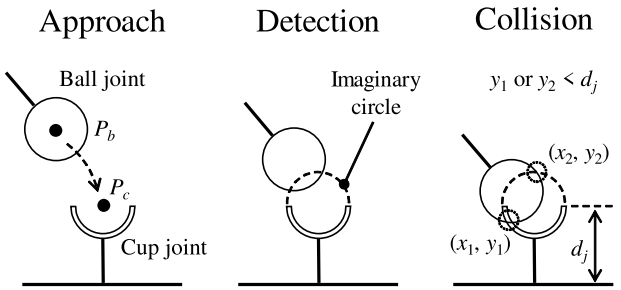

FIGURE 5. Collision between the ball and cup joints in the transition from the continuum state to the discrete state.

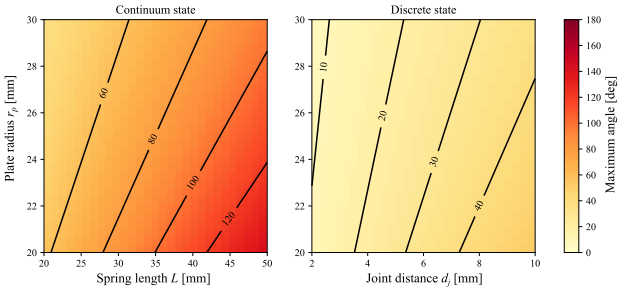

FIGURE 6. Visualization of the maximum bending angle determined by the collision of the two plates, shown in Fig. 3.

by (3) and Fig. 2.

$$P_{bj}(x, z) = (\lambda(1 - \cos\theta_c) - d_j \sin\theta_c, \quad \lambda \sin\theta_c - d_j \cos\theta_c) \tag{8}$$

The coordinate of the ball joint moves to $P_{cj}(x, z) = (0, d_j)$. Assuming that the cup joint has an imaginary circle with a radius of r_b, we can use the equation of circle-to-circle collision determination similar to (6). A collision between circles A and B means that the distance between the centers of A and B is smaller than the sum of the radii of A and B.

$$(x_A - x_B)^2 + (y_A - y_B)^2 \leq (r_A + r_B)^2 \tag{9}$$

We obtain the following equation from the coordinates and radii of the ball and cup joints:

$$(\lambda - \lambda\cos\theta_c - d_j \sin\theta_c)^2 + (\lambda \sin\theta_c - d_j \cos\theta - d_j)^2 \leq 4{r_b}^2 \tag{10}$$

When the left-hand side is less than the right-hand side in (10), the two circles collide and have two points of contact (middle part of Fig. 5). When the coordinate y of the collisions is smaller than d, the ball joint and the cup collide (right part of Fig. 5).

III. SIMULATION FOR COLLISIONS

A. RELATIONSHIP BETWEEN THE DESIGN PARAMETERS AND THE COLLISIONS

We investigate how the design parameters of the joints relate to the three collisions described in the previous section. Fig. 6 shows the maximum bending angles determined by the collision between the two plates given changes in the spring length L, joint length d_j, and plate radius r_p. The maximum bending angles θ_{cmax} and θ_{dmax} in the continuum and discrete states are calculated from (4) and (5), respectively. We set the ranges of L, d_j, and r_p to $20 < L < 50$, $2 < d_j < 10$, and $20 < r_p < 30$, respectively. The color bar indicates the maximum bending angle determined by the collision, with the darker colors indicating greater bend angles. The continuum state has a larger bending angle than the discrete state in the investigated range. Although the bending angle of the discrete state can be enlarged by increasing the distance d_j, the distance d_j must be less than half the length L. When $2d_j = L$, the robot section is in the discrete state.

Fig. 7 shows the maximum bending angle determined by the collision between the coil spring and the ball joint, as calculated from (7). The radius r_b of the ball joint is fixed to 3 mm, and the radius r_s of the coil spring is expressed by a ratio r_s/r_b of the two radii. We set the range of the spring length L from 20 mm to 50 mm, radius ratio r_s/r_b from 1.2 to 1.6, and joint distance d_j from 2 mm to 10 mm. We visualized the maximum bending angle determined by the spring-to-joint collision for different shape parameter values by using a contour map, where we compared it to the bending angle determined by the plate-to-plate collision by using contours. On the color bar, the darkest color indicates that the robot section can avoid the collision when it bends 180 degrees, and the lightest color indicates that the collision occurs when the robot section does not bend (i.e., 0 degrees). The three black solid contour lines show the maximum bending angle θ_{cmax} due to the plate-to-plate collision shown in Fig. 6; the plate radii r_p are 30 mm, 40 mm, and 50 mm, respectively, from the top to the bottom. When the distance d increases or the spring radius r_s decreases, the maximum bending angle θ_{cmax} decreases. As the spring length L increases, the maximum bending angle θ_{cmax} slightly increases. The contours, which show the maximum bending angle θ_{cmax} due to the plate-to-plate collision, help optimize the design parameters. The bending angle of the robot section can be maximized by designing the plate-to-plate and spring-to-joint collisions to occur at the same angle. For example, in the upper left part of Fig. 7, when $d_j = 8$ mm, $r_s/r_b = 1.5$, and $r_p = 20$, the two collisions occur simultaneously.

Fig. 8 numerically visualizes the robot end and ball joint positions to determine where the ball and cup joints collide. We set the joint distance d_j and the ball (or cup) radius r_b to 5 mm and 3 mm, respectively, and vary them within spring lengths L from 10 mm to 30 mm and bending angles θ_c from -45 degrees to 45 degrees. When the robot section is straight and L is the shortest, the coordinates of the ball and cup joints exactly match. The brightest dots represent the "Approach" state in Fig. 5. In this state, the ball and cup joints are separated from each other. The second darkest dots represent the "Detection" state in Fig. 5. In this state, the imaginary circle of the cup joint collides with the ball joint to determine whether the actual collision occurs. The darkest dots represent the state of "Collision" shown in Fig. 5. In this state, the circle of the ball joint collides with the semicircle

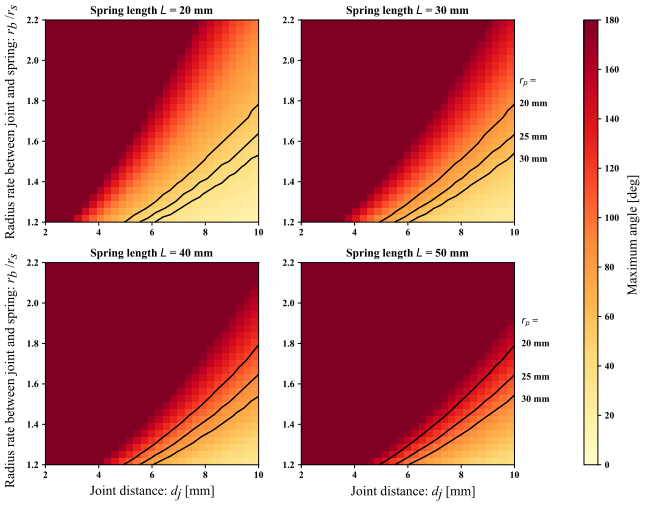

FIGURE 7. Visualization of the maximum bending angle determined by the collision between the joint and the spring, shown in Fig. 4. The contour lines show the maximum bending angle due to the collision between the two plates at each plate radius r_p in the left image of Fig. 6.

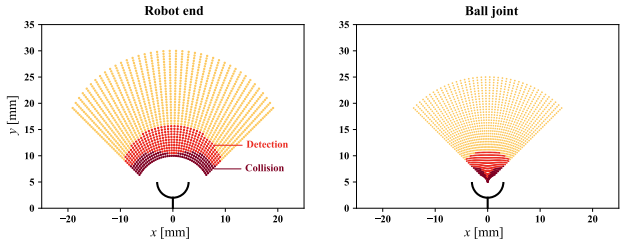

FIGURE 8. Visualization of the relationship between the positions of the robot end and the ball joint and the collision due to the two joints. The points represent the "Approach", "Detection", and "Collision" states shown in Fig. 5.

of the cup joint. The cup joint, in its actual size, is drawn at the origin. In both the robot end and the ball joint, collision is less likely to occur in the vicinity of $x = 0$, and the area in the collision that is slightly away from the vicinity becomes the maximum. Using this model, we can control the robot while avoiding the area where robot positioning is uncertain due to the collision between the ball and cup joints.

IV. EXPERIMENTS

A. EXPERIMENTAL VERIFICATION

To verify the three collision model, we built an experimental joint with a plastic ball and cup joint. The joint has a coil spring as a backbone in the center of the sections and is driven by three wires. To compare with the 2D collision model, the robot end was moved in the 2D plane with two of the three wires always set to the same length. In this experiment, we took several pictures while the robot was bent by wires. The angle and end position of the robot was measured from the images.

Fig. 9(a) shows a comparison of the plate-to-plate collision of the robot in the simulation with the real world. The joint distance d_j in the discrete state and the spring length L in the continuum state are 5 mm and 25 mm, respectively. We set the

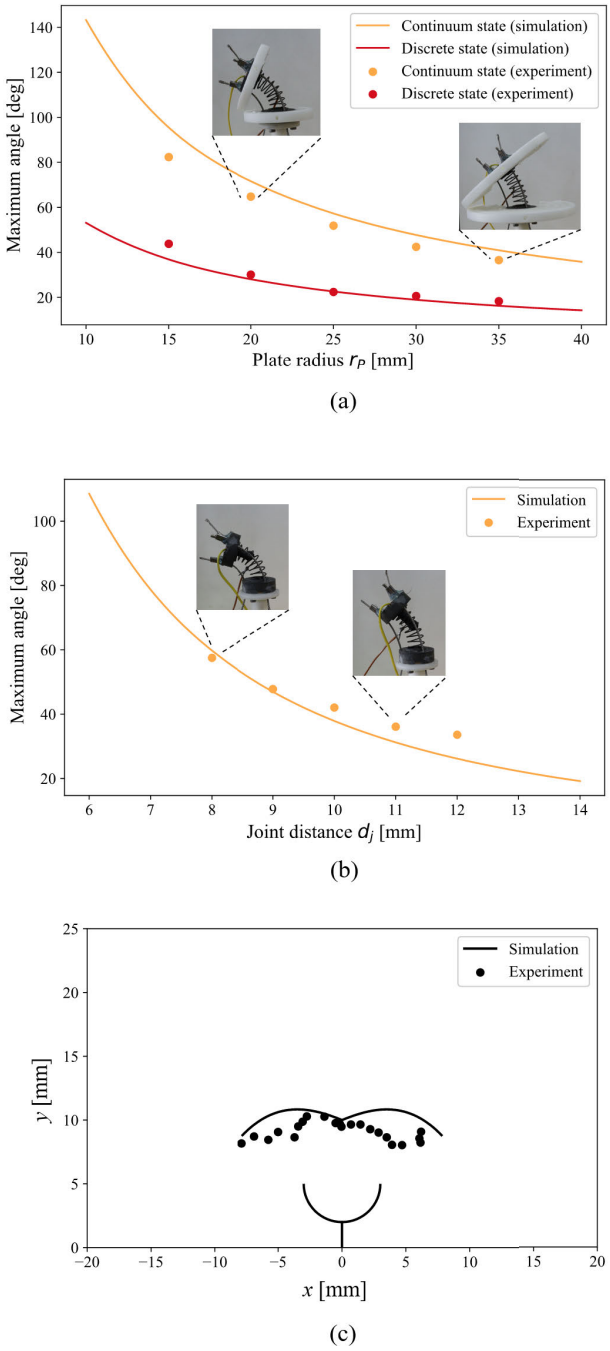

FIGURE 9. Experimental verification of the three collision models. (a) the plate-to-plate collision.(b) the joint-to-spring collision.(c) the ball-to-cup collision.

range of the plate radius r_P from 15 to 35 mm and measured the maximum angle of the robot end. The solid lines show the maximum angle simulated in (4) and (5), and the dots show the maximum angle measured in the experiment. We find that the simulation and the experiment are consistent in both the discrete and continuum states.

In the other two experiments, we use joints coated with conductive paint because detecting the collision of the small joints of the robot is difficult. An electrical cable is attached to the ball joint and the cup joint (or the spring) to detect

the collision. When a voltage is applied, the collision can be detected by the change in voltage. Fig. 9(b) shows a comparison of the joint-to-spring collision in the simulation with the real world. The spring length L is set to 25mm and the ball radius r_b is set to 3 mm. We measured the maximum angle determined by the collision between the ball joint and the spring when the joint distance d_j is changed from 8 to 12 mm. The simulation of the proposed collision model matches the real robot well, but minor errors arise because of manufacturing errors in the experimental joint.

Fig. 9(c) shows the experimental result with the simulation of the ball-to-cup collision model. The joint distance d_j and the ball (or cup) radius r_b are 5mm and 3 mm, respectively. We pulled three wires of the robot at a time when the spring length of 30 mm and the angle of -45 to 45 degrees simultaneously and measured the end position when the ball and the cup collided. The simulation, shown as solid lines, represents the boundary between the ''collision'' and ''detection'' state regions on the left side of Fig. 8. Minor errors between the simulation and the experiment are detectable, which probably arise because our model ignores the thickness of the cup joint and the axial compression of the backbone spring. The latter is known to be one of the causes of the breakdown of the constant curvature model in continuum robots [28].

B. VARIABLE STIFFNESS

We examine how the stiffness of the robot changes when the joint shifts from the continuum state to the discrete state. In a pre-experiment, we could not measure the stiffness of the robot with the plastic ball and cup joints used in Fig. 9 because of a large friction between the joints. Ideally, the use of a spherical rolling joint with bearing balls is desirable, but commercially available joints have the ball and cup connected to each other. Thus, we build a joint structure using a bearing and a cup (Fig. 10). Although the joint in the discrete state bends only in one plane, that in the continuum state bends in 3D space. The joint has a coil spring as a backbone in the center of the sections and is driven by three wires. Since the manipulator in the discrete state is ideally a rigid body, we use elastic elements with a non-linear force-displacement characteristic to change the stiffness. The stiffness depends on the torque at the joint, as is well known in the study of series elastic actuators [29]. We employed nitrile rubber O-rings (Fig. 11), which have nonlinear elasticity [30], [31]. Since the slope of the force-displacement curve of O-rings increases gradually, the stiffness by antagonistic wires increases as its displacement increases. One end of the stainless-steel wire is fixed to the end of the manipulator by an oval sleeve, while the other end is connected to a servo motor (S3003; Futaba, Japan) via an O-ring with the section diameter of 2mm and the outside diameter of 20 mm. The initial length of one section is 32 mm; when the length is 16 mm, the joints are entirely connected and shift to the discrete state. The section increases the stiffness of the whole structure by pulling the wires simultaneously. For example, when a load is applied to the robot end, the displacement under the same load decreases

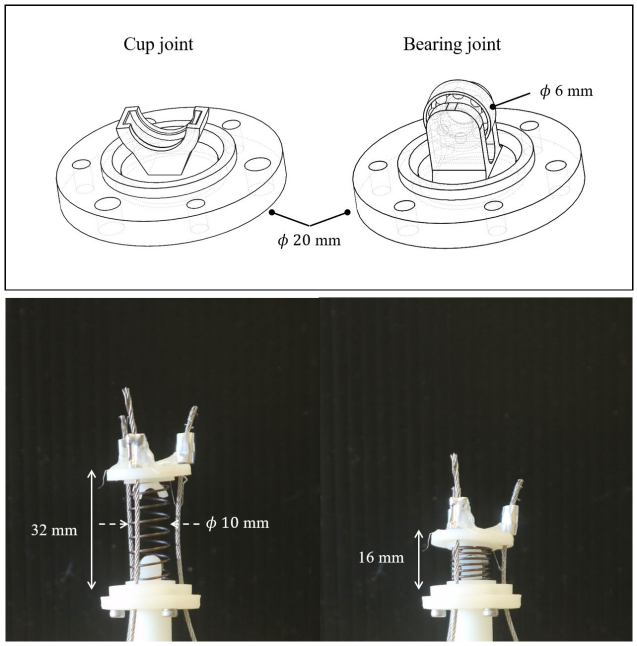

FIGURE 10. Prototype joint dislocation mechanism. For simplicity, we use a bearing and a cup in the joint.

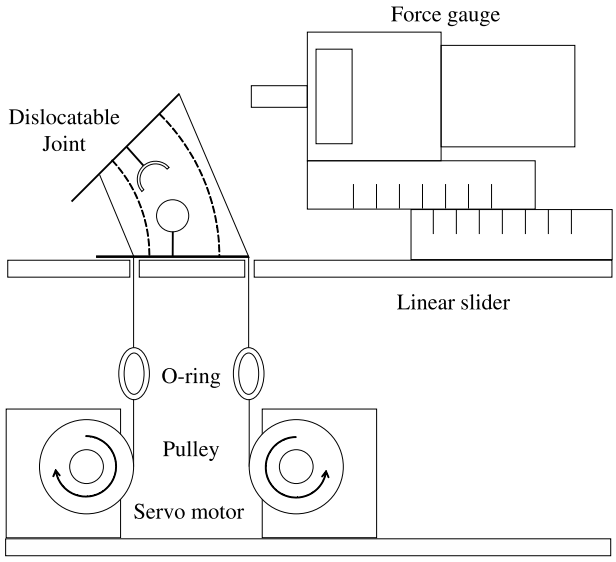

FIGURE 11. Experimental setup for measuring stiffness.

monotonically with the decrease in the length in the continuum state, and the stiffness increases. This is evident from the fact that the bending moment is reduced regardless of the compression of the backbone spring. A continuum robot without joints can pull the wire further, making it more rigid, but the shorter section length reduces the range of motion. The joint in the discrete state with constant section length can antagonize the nonlinear springs by pulling the wire further, which can greatly increase the stiffness.

Fig. 12 shows the stiffness characteristics of the joint when the displacement is applied through a force gauge. The tested direction is perpendicular to the axis of the ver-

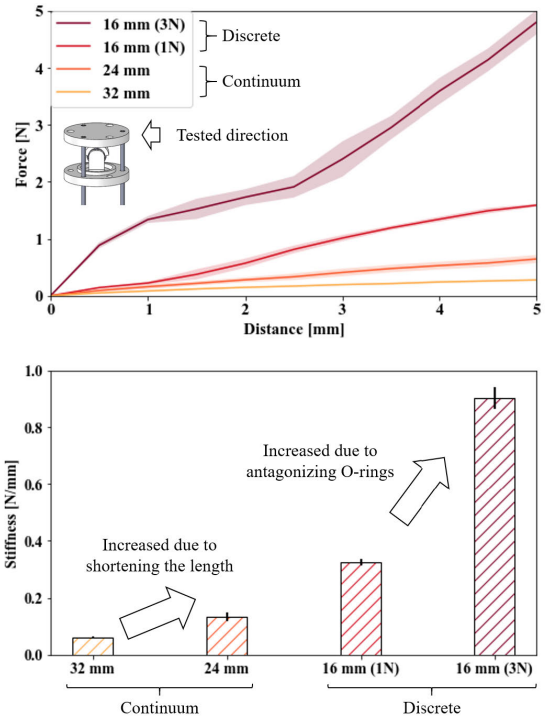

FIGURE 12. The joint dislocation mechanism enables active stiffness tuning of the manipulator. Using a force gauge mounted in the vertical direction to the long axis of the manipulator, we measure the stiffness under four conditions: section lengths of (i) 32 mm, (ii) 24 mm, (iii) 16 mm with a tension of 1 N, and (iv) 16 mm with a tension of 3 N. When a tension of 1 N is applied to each wire in (iii), the manipulator shifts to a discrete state. The upper graph shows a reaction force and displacement of the force gauge (light color shadings indicate SD from five tests of one displacement). The lower graph depicts the slopes of the four lines in the upper graph, as obtained by the least-squares method (error bars indicate SD from five tests).

FIGURE 13. Demonstration of the manipulator with three joint dislocation mechanisms. The upper image shows that the manipulator in the continuum state has a larger workspace than that in the discrete state. The lower image shows that the manipulator in the discrete state has a larger payload than that in the continuum state.

tically mounted joint and is also the edge in the triangle formed from the top view of the three wires. Note that the stiffness of the joint varies slightly depending on the tested direction because of a change of the distance projected from the side between the center of the joint and each wire. We adjust the wire tension to investigate the stiffness of three different section lengths of 16 mm, 24 mm, and 32 mm. When the section length is 32 mm, wires are pulled with very small tension to keep the manipulator posture. As the wire tension increases, the section length decreases. When about 1 N is applied to wires, the manipulator switches from the continuum state to the discrete state at a section length of 16 mm. Even when a greater tension is applied, the section length remains constant and the stiffness increases due to the antagonism of the O-rings. This test was conducted for four conditions, namely, section lengths of 16 mm with a tension of 3 N, 16 mm with a tension of 1 N, 24 mm, and 32 mm without a tension. When the force gauge is moved at 0.5 mm increments, the reaction force from the joint is measured five times for each condition. Fig. 12 shows that the reaction force increases linearly with respect to distance in the continuum state and a nonlinear curve in the discrete state. For a comparison of the values of stiffness for each section length, the inclines of the force-displacement curves are obtained using the least-squares method. We assume for simplicity that the nonlinear curve in the discrete state is a straight line. The stiffness of the joint, provided as an average of these trials, increases by a factor of five from the continuous state with the section length of 32 mm to the discrete state with the section length of 16 mm; it reached a maximum of 15 times at the pulling force of 3 N. Note that an increase of the stiffness in the continuum state depends mainly on the decrease section length, while that in the discrete state depends on the antagonism of the O-rings.

To intuitively understand the benefits of the proposed mechanism, we build a prototype manipulator with three sections, which are driven by three wires. The upper part of Fig. 13 shows the difference in the range of motion of the robot in the continuous and discrete states. In the continuum state, the manipulator can turn nearly 270 degrees, but in the discrete state, it can turn only about 90 degrees. This is mainly because the range of motion is limited by the plate-to-plate collision. The lower part of Fig. 13 shows the manipulator in the continuum and discrete states of lifting the weight. In the continuum state, the manipulator buckles left and right even with a light load of about 50 g. In the discrete state, the manipulator lifts a load of 250 g without buckling. These results show that each state has distinct advantages. In the continuous state, the manipulator has a large bending radius and reachable area; in the discrete state, it can handle a large payload because there is no buckling due to compliance.

V. CONCLUSION

To demonstrate the potential of a joint dislocation mechanism, we built a wire-driven manipulator that has a dislocatable joint comprising a set of cup and ball joints. The manipulator works in the continuum or discrete state through the control of the position and tension of the wires. This study shows that both states have unique advantages. Although the robot in the continuum state has compliance and a large workspace, it does not have rigid links to support its body and cannot lift heavy objects. The robot in the discrete state has a large payload, but the range of bending motion is narrow due to the narrow distance between the upper and lower section plates. In robot manipulators, both properties are needed depending on the problem. For example, grasping a fragile object by wrapping around it requires compliance and a wide range of motion, whereas lifting and manipulating such an object requires a large payload and precision. Comprehensive experiments for compliance, range of motion, payload, and precision would highlight the benefits of our idea. A summary of our research is shown in the supplementary video.

We built a model of the manipulator joint and considered three cases of collisions: (i) plate and plate, (ii) joint and spring, and (iii) ball and cup joints. The model showed that the desired bending angle in both continuum and discrete states can be achieved by changing the robot's shape parameter. The model also visualized the region of instability in the positioning of the manipulator determined by the collision between the ball and cup joints, which will be helpful in the motion planning of the manipulator in the future. The stiffness of the prototype manipulator at different robot lengths and wire tension was tested, and we found that it can be improved by up to a factor of 15. In this experiment, due to the output limit of the servomotor, the wire could only be pulled with a maximum force of 3 N. However, the stiffness of the manipulator can be further increased by applying a higher wire tension. A promising area of future investigation is to understand how the stiffness can be varied by modeling the O-rings and backbone springs.

There are many opportunities for further developments. For example, the collision model can be expressed in geometry; however, the actual system will involve gravity and axial compression which require the dynamics of flexible beams. We will extend our model with additional physical effects. In the continuum state the wires in the manipulator follow a constant curvature model, but in the discrete state they follow a straight line due to large tension. Thus, the manipulator operates with different control laws depending on the two states. The prototype joint uses a ball bearing instead of a spherical rolling joint, so there is one less degree of freedom in the discrete state. We will build a new cup joint with bearing balls and a spherical retainer. Another opportunity for development is optimizing the joint geometry. For example, when the manipulator switches from the continuum state to the discrete state with a heavy load, the two joints may misalign and not join together well. Investigating the coupling of the two joints at high loads will lead to further understanding and practical application of our joint dislocation mechanism.

REFERENCES

[1] G. A. Pratt and M. M. Williamson, "Series elastic actuators," in *Proc. IEEE/RSJ Int. Conf. Intell. Robots Syst. (IROS)*, vol. 1, Aug. 1995, pp. 399–406.
[2] *HEBI Robotics*. Accessed: Dec. 20, 2020. [Online]. Available: https://www.hebirobotics.com/
[3] *Rethink Robotics*. Accessed: Dec. 20, 2020. [Online]. Available: https://www.rethinkrobotics.com/
[4] D. B. Camarillo, C. F. Milne, C. R. Carlson, M. R. Zinn, and J. K. Salisbury, "Mechanics modeling of tendon-driven continuum manipulators," *IEEE Trans. Robot.*, vol. 24, no. 6, pp. 1262–1273, Dec. 2008.
[5] I. A. Gravagne, C. D. Rahn, and I. D. Walker, "Large deflection dynamics and control for planar continuum robots," *IEEE/ASME Trans. Mechatronics*, vol. 8, no. 2, pp. 299–307, Jun. 2003.
[6] H.-S. Yoon and B.-J. Yi, "A 4-DOF flexible continuum robot using a spring backbone," in *Proc. Int. Conf. Mechatronics Automat. (ICMA)*, Aug. 2009, pp. 1249–1254.
[7] M. B. Pritts and C. D. Rahn, "Design of an artificial muscle continuum robot," in *Proc. IEEE Int. Conf. Robot. Automat.*, vol. 5, Apr./May 2004, pp. 4742–4746.
[8] G. Chen, M. T. Pham, and T. Redarce, "A guidance control strategy for semi-autonomous colonoscopy using a continuum robot," in *Recent Progress in Robotics: Viable Robotic Service to Human*. Berlin, Germany: Springer, 2007, pp. 63–78.
[9] A. Bartow, A. Kapadia, and I. D. Walker, "A novel continuum trunk robot based on contractor muscles," in *Proc. WSEAS Int. Conf. Signal Process. Robot., Automat.*, 2013, pp. 181–186.
[10] H. M. Jaeger, "Celebrating soft matter's 10th anniversary: Toward jamming by design," *Soft Matter*, vol. 11, no. 1, pp. 12–27, 2015.
[11] C. Laschi, B. Mazzolai, and M. Cianchetti, "Soft robotics: Technologies and systems pushing the boundaries of robot abilities," *Sci. Robot.*, vol. 1, no. 1, Dec. 2016, Art. no. eaah3690.
[12] N. G. Cheng, M. B. Lobovsky, S. J. Keating, A. M. Setapen, K. I. Gero, A. E. Hosoi, and K. D. Iagnemma, "Design and analysis of a robust, low-cost, highly articulated manipulator enabled by jamming of granular media," in *Proc. IEEE Int. Conf. Robot. Automat.*, May 2012, pp. 4328–4333.
[13] M. Cianchetti, T. Ranzani, G. Gerboni, I. De Falco, C. Laschi, and A. Menciassi, "STIFF-FLOP surgical manipulator: Mechanical design and experimental characterization of the single module," in *Proc. IEEE/RSJ Int. Conf. Intell. Robots Syst. (IROS)*, Nov. 2013, pp. 3576–3581.
[14] Y.-J. Kim, S. Cheng, S. Kim, and K. Iagnemma, "A novel layer jamming mechanism with tunable stiffness capability for minimally invasive surgery," *IEEE Trans. Robot.*, vol. 29, no. 4, pp. 1031–1042, Aug. 2013.
[15] A. Pettersson, S. Davis, J. O. Gray, T. J. Dodd, and T. Ohlsson, "Design of a magnetorheological robot gripper for handling of delicate food products with varying shapes," *J. Food Eng.*, vol. 98, no. 3, pp. 332–338, Jun. 2010.
[16] O. Ashour, C. A. Rogers, and W. Kordonsky, "Magnetorheological fluids: Materials, characterization, and devices," *J. Intell. Mater. Syst. Struct.*, vol. 7, no. 2, pp. 123–130, Mar. 1996.
[17] C. Cao and X. Zhao, "Tunable stiffness of electrorheological elastomers by designing mesostructures," *Appl. Phys. Lett.*, vol. 103, no. 4, Jul. 2013, Art. no. 041901.
[18] N. G. Cheng, A. Gopinath, L. Wang, K. Iagnemma, and A. E. Hosoi, "Thermally tunable, self-healing composites for soft robotic applications," *Macromol. Mater. Eng.*, vol. 299, no. 11, pp. 1279–1284, Nov. 2014.
[19] M. A. McEvoy and N. Correll, "Thermoplastic variable stiffness composites with embedded, networked sensing, actuation, and control," *J. Compos. Mater.*, vol. 49, no. 15, pp. 1799–1808, Jun. 2015.
[20] K. Suzumori, S. Wakimoto, K. Miyoshi, and K. Iwata, "Long bending rubber mechanism combined contracting and extending fluidic actuators," in *Proc. IEEE/RSJ Int. Conf. Intell. Robots Syst. (IROS)*, Nov. 2013, pp. 4454–4459.
[21] E. I. S. Flores, M. I. Friswell, and Y. Xia, "Variable stiffness biological and bio-inspired materials," *J. Intell. Mater. Syst. Struct.*, vol. 24, no. 5, pp. 529–540, Mar. 2013.
[22] T. Motokawa, "Connective tissue catch in echinoderms," *Biol. Rev.*, vol. 59, no. 2, pp. 255–270, May 1984.

[23] I. C. Wilkie, "Mutable collagenous tissue: Overview and biotechnological perspective," in *Echinodermata*. Berlin, Germany: Springer, 2005, pp. 221–250.
[24] K. V. Kardong, "Kinesis of the jaw apparatus during swallowing in the cottonmouth snake, agkistrodon piscivorus," *Copeia*, vol. 1977, no. 2, pp. 338–348, 1977.
[25] H.-C. Fu, J. D. L. Ho, K.-H. Lee, Y. C. Hu, S. K. W. Au, K.-J. Cho, K. Y. Sze, and K.-W. Kwok, "Interfacing soft and hard: A spring reinforced actuator," *Soft Robot.*, vol. 7, no. 1, pp. 44–58, Feb. 2020.
[26] Y.-S. Seo, S. J. Cho, J.-Y. Lee, C. Park, U. Kim, S. Lee, B. Kim, C. Park, and S.-H. Song, "Human-mimetic soft robot joint for shock absorption through joint dislocation," *Bioinspiration Biomimetics*, vol. 15, no. 1, Nov. 2019, Art. no. 016001.
[27] R. J. Webster and B. A. Jones, "Design and kinematic modeling of constant curvature continuum robots: A review," *Int. J. Robot. Res.*, vol. 29, no. 13, pp. 1661–1683, Nov. 2010.
[28] D. C. Rucker, *The Mechanics of Continuum Robots: Model-Based Sensing and Control*. Nashville, TN, USA: Vanderbilt Univ., 2011.
[29] A. Albu-Schaffer, O. Eiberger, M. Grebenstein, S. Haddadin, C. Ott, T. Wimbock, S. Wolf, and G. Hirzinger, "Soft robotics," *IEEE Robot. Autom. Mag.*, vol. 15, no. 3, pp. 20–30, Sep. 2008.
[30] M. Jantsch, S. Wittmeier, K. Dalamagkidis, A. Panos, F. Volkart, and A. Knoll, "Anthrob—A printed anthropomimetic robot," in *Proc. 13th IEEE-RAS Int. Conf. Hum. Robots (Humanoids)*, Oct. 2013, pp. 342–347.
[31] K. Kawaharazuka, K. Kawasaki, M. Inaba, S. Makino, K. Tsuzuki, M. Onitsuka, Y. Nagamatsu, K. Shinjo, T. Makabe, Y. Asano, and K. Okada, "Component modularized design of musculoskeletal humanoid platform Musashi to investigate learning control systems," in *Proc. IEEE/RSJ Int. Conf. Intell. Robots Syst. (IROS)*, Nov. 2019, pp. 7300–7307.

AYATO KANADA (Member, IEEE) received the Ph.D. degree in mechanical engineering from the Toyohashi University of Technology, Japan, in 2020. He is currently an Assistant Professor with the Department of Mechanical Engineering, Kyushu University, Fukuoka, Japan.

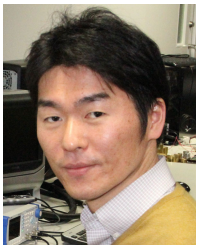

TOMOAKI MASHIMO (Member, IEEE) received the Ph.D. degree in mechanical engineering from the Tokyo University of Agriculture and Technology, Fuchu, Japan, in 2008. From 2008 to 2010, he was a Robotics Researcher with the Robotics Institute, Carnegie Mellon University, Pittsburgh, PA, USA. In 2011, he was an Assistant Professor (tenure-track) with the Toyohashi University of Technology, Toyohashi, Japan, where he became an Associate Professor, in 2016. His research interests include piezoelectric actuators and the robotic applications.